High-efficiency photonic crystal microlaser integrated with a passive waveguide

Hideki Watanabe and Toshihiko Baba

Yokohama National University, Department of Electrical and Computer Engineering
79-5 Tokiwadai, Hodogayaku, Yokohama 240-8501, Japan

Core Research for Evolutional Science and Technology (CREST),
Japan Science and Technology (JST) Agency, Sanbancho Building 5,
Sanbancho, Tiyodaku, Tokyo 102-0075, Japan

Email: baba@ynu.ac.jp

Abstract: A GaInAsP photonic crystal slab microlaser with an integrated passive waveguide was fabricated by a MOCVD butt-joint regrowth process. The boundary between the active and passive regions was optimized for high light transmission. In addition, the edge of the waveguide was designed to output a narrow beam, and the light detection was improved. Consequently, a maximum output power of 0.17 mW was obtained with a differential quantum efficiency of 20%, which would increase to more than 40% under ideal detection conditions.

OCIS codes: (140.5960) Semiconductor lasers; (230.3990) Microstructure devices.

References and links

1. K. Nozaki, S. Kita, and T. Baba, "Room temperature continuous wave operation and controlled spontaneous emission in ultrasmall photonic crystal nanolaser," Opt. Exp. **15**, 7506–7514 (2007).
2. K. Srinivasan, P. Barclay, O. Painter, J. Chen, A. Y. Chuo, and C. Gmachl, "Experimental demonstration of a high quality factor photonic crystal," Appl. Phys. Lett. **83**, 1915–1917 (2003).
3. M. Nomura, S. Iwamoto, K. Watanabe, N. Kumagai, Y. Nakata, S. Ishida, and Y. Arakawa, "Room temperature continuous-wave lasing in photonic crystal nanocavity," Opt. Exp. **14**, 6308–6315 (2006).
4. T. Baba, N. Fukaya, and J. Yonekura, "Observation of light transmission in photonic crystal waveguides with bends," Electron. Lett. **35**, 654–655 (1999).
5. E. Kuramochi, M. Notomi, S. Hughes, A. Shinya, T. Watanabe, and L. Ramunno, "Disorder-induced scattering loss of line-defect waveguides in photonic crystal slabs," Phys. Rev. B **72**, 161318(R) (2005).
6. I. K. Hwang, S. K. Kim, J. K. Yang, S. H. Kim, S. H. Lee, and Y. H. Lee, "Curved-microfiber photon coupling for photonic crystal light emitter," Appl. Phys. Lett. **87**, 131107 (2005).
7. Y. Park, S. Kim, C. Moon, H. Jeon, and H. J. Kim, "Butt-end fiber coupling to a surface-emitting Gamma-point photonic crystal band edge laser," Appl. Phys. Lett. **90**, 171115 (2007).
8. H. Watanabe and T. Baba, "Active/passive-integrated photonic crystal slab microlaser," Electron. Lett. **42**, 695–696 (2006).
9. T. Ide, J. Hashimoto, K. Nozaki, E. Mizuta, and T. Baba, "InP etching by HI/Xe inductively coupled plasma for photonic-crystal device fabrication," Jpn. J. Appl. Phys. **45**, L102–L104 (2006).
10. P. Kramper, M. Agio, C. M. Soukoulis, A. Birner, F. Müller, R. B. Wehrspohn, and V. Sandoghdar, "Highly directional emission from photonic crystal waveguides of subwavelength width," Phys. Rev. Lett. **92**, 113903 (2004).

Semiconductor photonic crystal (PC) slabs having a photonic bandgap and unique dispersion characteristics have been studied for various device applications including active devices such as lasers [1-3] and passive devices such as waveguides [4,5]. For sophisticated optical signal processing, these devices should be integrated on a chip. However, it has been difficult to integrate active and passive devices in a PC slab. For this reason, there have been few reports of light extraction from PC microlasers and little quantitative evaluation of their efficiencies;

#90817 - $15.00 USD Received 12 Dec 2007; revised 24 Jan 2008; accepted 1 Feb 2008; published 12 Feb 2008

only the evanescent coupling into external fibers and the vertical beaming of light output have been studied [6,7]. Previously, we have reported fabrication of a PC slab with integrated active and passive regions using a metal organic chemical vapor deposition (MOCVD) butt-joint regrowth technique and succeeded in extracting laser light from its passive waveguide [8]. In that study, a line-defect PC microlaser and a line-defect PC waveguide were formed in the active and passive regions, respectively. In an optical pumping experiment at room temperature, we measured a maximum output power of 5.5 μW. Using an estimate of the effective pump power, we computed the differential quantum efficiency η_d to be 8%. Clearly these values leave room for improvement. In the present Letter, we report a much higher output power and efficiency. They were obtained by optimizing the active/passive boundary (accounting for the difference in refractive indices), by narrowing the radiation pattern of the output light via control of the modal field along the waveguide edge, and by improving the light detection using a lensed fiber.

The active/passive-integrated wafer was formed out of InP using a regrowth technique. The active region consisted of six sets of GaInAsP quantum wells, barrier layers, and separate confinement heterostructure layers. The total thickness of all these layers was 210 nm and its photoluminescence spectrum peaked at a wavelength of 1.55 μm. The passive region consisted of a 1.30-μm-peak GaInAsP bulk layer, whose thickness was also 210 nm. The PC slab was fabricated using *e*-beam lithography, HI/Xe inductively coupled plasma etching [9], and HCl wet etching. The PC airholes were arranged in a triangular lattice with a lattice constant a of 450 nm. A straight line defect consisting of one row of missing airholes (called a "W1 waveguide") extended from the active to the passive regions to function as a laser cavity and as a waveguide, respectively. The airhole diameter in the active region $2r_a$ was fixed at 250 nm and that in the passive region $2r_p$ was varied from sample to sample. Figure 1 shows scanning electron microscope images of the fabricated device. The two regions were connected together with negligible position error in the vertical direction. A projection formed at the boundary during the regrowth process, but its height was less than 10 nm so that light scattering from it was negligible. In the measurement, 0.98-μm-wavelength pulsed laser light with a duty cycle of 0.075% and a spot diameter of 6.5 μm was focused onto the top surface of the active region. Lasing occurred in the active region due to the low group velocity near the photonic band edge of the W1 waveguide mode, and the laser light was extracted through the passive waveguide. Output light was directly collected by a multimode fiber GI50 and characterized by an optical spectrum analyzer.

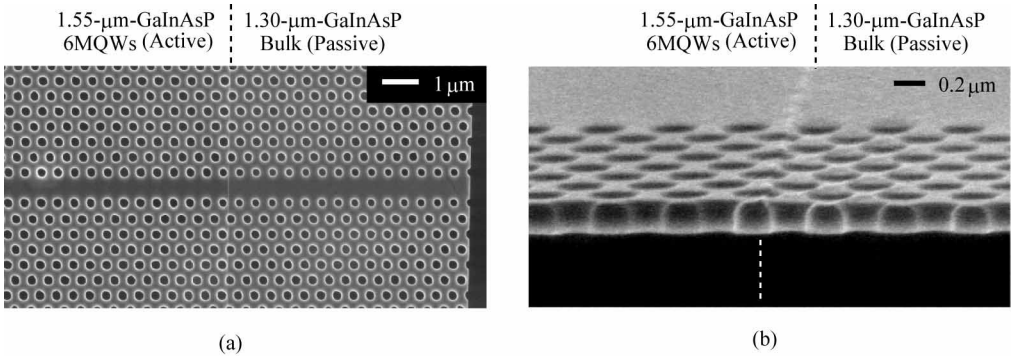

Fig. 1. Scanning electron microscope images of the fabricated microlaser and waveguide in the GaInAsP active/passive-integrated PC slab. (a) Top view. (b) Cross-sectional view.

#90817 - $15.00 USD Received 12 Dec 2007; revised 24 Jan 2008; accepted 1 Feb 2008; published 12 Feb 2008

Due to the differing material compositions and refractive indices of the active and passive regions, a modal mismatch occurs when $r_a = r_p$. Average values of the refractive indices of the active and passive slabs at a wavelength of 1.55 μm were estimated to be 3.39 and 3.45, respectively. Therefore, if the same PC design is employed in both regions, the photonic band in the passive region shifts to lower frequencies. If r_p is changed relative to r_a, this band shift can be controlled. Figure 2(a) shows the dependence of the photonic band on the ratio r_p/r_a calculated by a plane-wave expansion method and the modal field calculated by a finite-difference time-domain (FDTD) method. Meanwhile Fig. 2(b) graphs show the output power determined by the FDTD method. Because fine tuning of the value of r_p was limited by the finite Yee cells in the FDTD calculation, we fixed $r_p = r_a$ and the tuning of r_p was instead performed by varying the slab index during the calculations. This is equivalent to varying r_p, at least over a narrow tuning range, because the band shape does not change and its frequency merely shifts when either r_p or the index is varied. As the ratio r_p/r_a increases from unity, so that the modal mismatch at the boundary is reduced, the output power is enhanced until a maximum is attained at $r_p/r_a = 1.07$. When $r_p/r_a > 1.07$, laser light cannot be extracted from the waveguide owing to its cutoff. In Fig. 2(b), the dots graph shows the relative output power measured for many devices with different values of $2r_p$ using an as-cleaved fiber having a numerical aperture (NA) of 0.20. The experimental dots roughly follow the trends in the theoretical calculation (solid curve). The large fluctuations in the experimental values might be caused by uncertainties in the position of the waveguide edge, which was formed by simply cleaving it.

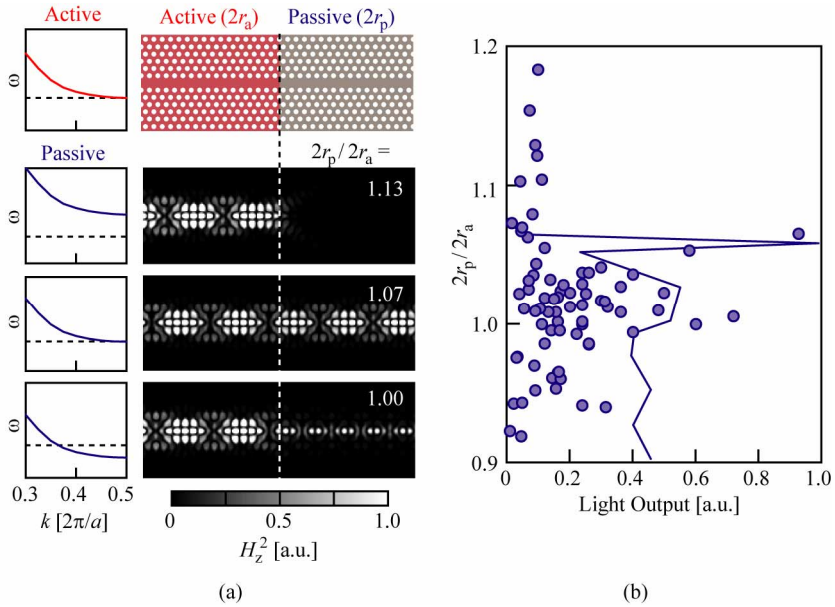

Fig. 2. Dependence of the light output on the airhole radius ratio r_p/r_a. (a) Calculated photonic bands (angular frequency ω versus wavenumber k) of the passive waveguide and the resulting intensity distributions for light propagation. (b) Theoretical (solid curve) and experimental (dots) plots of the output optical power.

It has previously been reported that the position of the waveguide edge relative to the PC structure significantly influences the radiation pattern of the output light [10]. Figure 3 summarizes the dependence of the radiation pattern and measured output power on the edge position, as calculated by the FDTD method. Looking back toward the device, the radiation

#90817 - $15.00 USD Received 12 Dec 2007; revised 24 Jan 2008; accepted 1 Feb 2008; published 12 Feb 2008

intensity orients in the center direction when the end airholes of the PC slab are located on the edge of the waveguide. But is the pattern almost splits into two and rotates by ±40° when the last airholes are well away from the end of the waveguide. The explanation is that, in the former case, a surface mode is excited by the waveguide and the modal distribution on the waveguide edge rapidly expands, resulting in a narrow beam divergence. In the calculation of the output power in Fig. 3, an NA of 0.56 resulted in the solid curve while an NA of 0.20 gave the dashed curve. The experimental plots in the same figure were obtained using a lensed fiber having an NA of 0.56. The intensity strongly depends on *d* which is the distance from the waveguide edge to the center of the end air holes. For either value of NA, the calculated output power in Fig. 3(b) varies by about a factor of 2, which could explain the large fluctuations in the experimental data in Fig. 2(b).

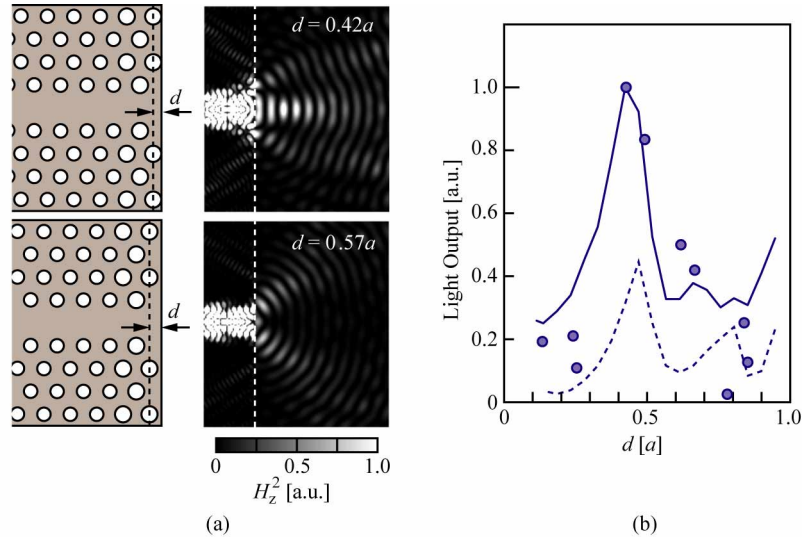

Fig. 3. Dependence of the light output on the edge structure of the passive waveguide. Dashed line shows the waveguide edge. Holes of end 3 rows are expanded by 20% to simulate the fabricated devices. (a) Calculated radiative distribution. (b) Theoretical (curves) and experimental (dots) plots of the output optical power as a function of the distance *d* from the edge of the waveguide to the center of the last airholes.

Figure 4 shows the characteristics of the device that had the highest output and pump powers in our measurement setup. The near-field beam spots photographed in Fig. 4(b) show that laser light is being extracted from the waveguide facet. Compared with our previous experiment using as-cleaved fiber, the detection has been improved by using a lensed fiber. The output power was now measured to be as large as 0.17 mW. To our knowledge, this is the first time that a practical value for the output power of a PC microlaser has been demonstrated. The intensity of the laser mode was 40 dB above the background level. The horizontal axis in Fig. 4(c) indicates the effective pump power estimated by considering both the overlap efficiency $\eta_{overlap}$ of the pump light with the laser area and the absorption efficiency η_{abs} of the pump light by the active layer. For the horizontal axis labeled "(A)," the laser area was defined as the space sandwiched between the innermost airholes of the line defect. In that case, $\eta_{overlap}$ is calculated to be 11%. For the other axis labeled "(B)," the laser area was estimated from the effective modal width W_{eff} calculated using $\int_{-\infty}^{\infty} dx \int_{z}^{z+a} dz \mu H_z^2 = \frac{1}{2} \mu H_{z\,max}^2 a W_{eff}$, where *x* and *z* denote the lateral and propagation

#90817 - $15.00 USD Received 12 Dec 2007; revised 24 Jan 2008; accepted 1 Feb 2008; published 12 Feb 2008

directions, respectively, and μH_z^2 is the modal energy density where μ is the permeability of the slab and H_z is the *z*-component of the magnetic field. In this case, $\eta_{overlap}$ becomes 33%. On the other hand, η_{abs} is estimated[16] to be 30% when the absorption length and coefficient are assumed to be 210 nm and 20000 cm^{-1}, respectively. Effective threshold powers P_{th} for cases (A) and (B) are 0.1 mW and 0.2 mW, and the differential quantum efficiencies η_d are 60% and 20%, respectively. In our previous study, [6] η_d was estimated to be 8% for P_{eff} (A) and so we have now managed to increase it eight-fold in value. Even in case (B), η_d remains large enough to claim as a value of laser. Because the detection efficiency of the lensed fiber is calculated by the FDTD method to be 45%, the value of η_d for P_{eff} (B) seems more reasonable than that for P_{eff} (A). But even in that case, η_d for the total light output including undetectable components must still be higher than 40%. In any event, η_d estimated from the ratio of the irradiated and detected powers is as low as 1.5%, mainly due to the small values of $\eta_{overlap}$ and η_{abs}. Note however that the value of $\eta_{overlap}$ could be greatly improved if line-shape pump light were used.

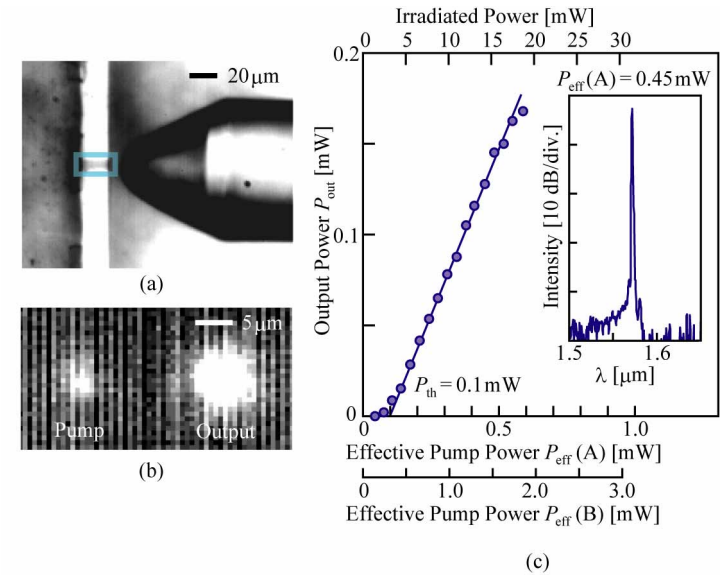

Fig. 4. Laser characteristics. (a) Device (blue square) and lensed fiber with a numerical aperture of 0.56 for detection (right side). (b) Near-field images of the laser beam cross sections. (c) Output versus input powers of the best device for two different calculations (A and B) of the pump spot size. The inset shows the measured spectral intensity of the output beam.

In conclusion, we have improved the operation of an active/passive-integrated PC microlaser fabricated using an MOCVD butt-joint regrowth technique. By optimizing both the active/passive boundary and the waveguide edge, and by improving the detection technique, the output power and differential quantum efficiency were measured to be as high as 0.17 mW and 20%, respectively. The differential quantum efficiency would increase to more than 40% under ideal detection conditions. These are promising values for future applications of ultrasmall lasers in photonic integrated circuits.

#90817 - $15.00 USD Received 12 Dec 2007; revised 24 Jan 2008; accepted 1 Feb 2008; published 12 Feb 2008